Hindawi
International Transactions on Electrical Energy Systems
Volume 2023, Article ID 3992158, 10 pages
https://doi.org/10.1155/2023/3992158

Research Article

Damping of Low-Frequency Oscillations in a Power System, Based on Multiple-Model Optimal Control Strategy

Elahe Pagard, Shahrokh Shojaeian, and Mohammad Mahdi Rezaei

Department of Electrical Engineering, Khomeinishahr Branch, Islamic Azad University, Isfahan, Iran

Correspondence should be addressed to Shahrokh Shojaeian; shojaeian@iaukhsh.ac.ir

Received 17 September 2022; Revised 26 November 2022; Accepted 14 December 2022; Published 9 January 2023

Academic Editor: Akshay Kumar Saha

This paper proposes a new control strategy based on multimodel linear optimization control (MMLOC) to damp power system low-frequency oscillations (LFO) faster. The multimodel control strategy is used to anticipate synchronous generator dynamic behavior and linear optimization control for generating a control signal uncomplicatedly. The third-order model of synchronous machine is considered for each of the models. The probability of each model's validity is evaluated from the difference between model outputs and the same actual power system outputs via the Bayesian approach. To improve the postfault dynamics of the case study power system, which contains a static VAR compensator, a linear optimal controller (LOC) is designed. The 8^{th} order model of the machines is used in simulations to represent the plant as accurately as possible.

1. Introduction

Nowadays, the power system stability issue and the effect of low-frequency oscillations (LFO) on large and modern power systems, which include distributed generators and high voltage DC lines, have become more important than ever. In addition, small and plenty of renewable energy sources are continuously growing up, and then, the low inertia of these generators adversely affects the overall stability of the power system [1–6]. To mitigate this challenge, many investigations based on different linear and nonlinear control methods have been made in recent decades. In [3] using eigenvalue analysis have been investigated LFO in a power system. In many references, LFO in power systems has been limited to using a power system stabilizer (PSS). In power systems including flexible transmission systems (FACTs), these devices must be coordinated with PSS to better control the transient behavior of the power system. Hence, in some previous studies, PSS restructuring has been carried out using optimization algorithms to achieve better performance in system stabilization. The optimization techniques Coyote algorithm and whale algorithm are used in [7, 8], respectively. In some other studies, the design of the PSS has been modified to improve LFO such as the fractional-order PID-PSS method [9] and the lead-lag control method [10], and in other papers, the new designs for PSS have been introduced on the power system [11, 12]. Due to the nonlinear characteristics of the electronic power converter, LFO is easily created. Improvement oscillations attenuation of a virtual synchronous machine connected to a voltage source converter (VSM) has been investigated using the virtual power system stabilizer (VPSS) in [3, 13]. A study of LFO in the power system shows that the investigation of nonlinear factors that change with time, which occurs due to fault scenarios, can be analyzed the path eigenvalues [2] and can be improved [14]. The multimodel method is used to estimate machine and system dynamics in postfault conditions. This method has been investigated and simulated using the PI controller in [15]. Other samples of applying a multimodel approach to damp of LFO can be found in [16–18].

Due to the nonlinear nature of modern and interconnected power systems, the methods based on nonlinear control have been discussed in many papers [19–30]. The sliding mode (SM) control in combination with fuzzy control has been used in [20, 21]. Some other papers have applied the various order SM controllers to damp LFOs [22–27]. These papers, in some cases, have proposed the

fractional-order SM controllers [22, 23] and the higher-order SM controller [26, 27]. In [29], a SM control is used on an extended state observer to improve LFOs. Nonlinear control methods show better performance for LFO damping, but their implementation has certain complexities. In some papers, nonlinear control methods have been combined with linear methods to take advantage of both. The suggestion of [31] is to combine the desirable features of the PID controller and many optimal effective features of the SM controller to eliminate the chattering. In order to produce the best control signal for the excitation system, a robust SM-PID design has been performed on a single machine infinite bus (SMIB) system to increase its stability. In [32], combining PID and SM controllers have been proposed to achieve the advantages of both controllers. Also, the linear optimal control (LOC) method for damping LFOs in [33–35] is discussed. To examine the other practice of incorporating linear and nonlinear control methods, in this paper, the combination of LOC and the multiple-model control (MMC) strategy is proposed and implemented on a single machine system. The system postfault behavior is analyzed and compared with conventional SM control. Since the SM control which have been studied in other references, are very effective in controlling LFOs. Despite the fact that nonlinear control methods are effective in damping low-frequency oscillations, the structural complexity and implementation problems of these methods are considered a major drawback in the power industry. Therefore, we intend to increase the accuracy of the proposed control strategy to nonlinear control methods.

2. The MMC Strategy

The block diagram of MMC strategy is shown in Figure 1. In this strategy, multiple identifier models are used to model dynamics behavior of synchronous generator. The models have been composed based on different set points of the synchronous generator. Each model estimates plant parameters, and then, the differences between the estimated and actual values are calculated. According to Figure 1, the MMC strategy scheme consists of three main blocks and two sub-blocks. The main parts are the plant, the model bank, and the control bank, and the subparts include the weight calculation block and the incorporation block.

2.1. Studied Power System. A SMIB power system shown in Figure 2 is used in this paper. The synchronous generator has been connected to the infinite bus via double transmission lines. A static var compensator (SVC) is located in the middle of one of the lines.

2.2. Calculation of Model Weights. The probability of each model is calculated for each synchronous generator model, according to the difference in the measured and calculated angular speed at each time. Then, based on the calculated errors and calculated probabilities in the previous step for each model, the new probabilities have been computed. A model that is less different from the plant should have a greater impact on to control of the plant. The Bayes recursive theory has been used to achieve this goal. At the k^{th} time step, the weights of each model are computed from

$$P_{i,k} = \frac{\exp\left(-1/2e_{i,k}^{T} C_{fe_{i,k}}\right) P_{i,k} - 1}{\sum_{j=1}^{N} \exp\left(-1/2e_{i,k}^{T} C_{fe_{i,k}}\right) P_{i,k} - 1}, \quad (1)$$

$$e_{i,k} = y_k - y_{i,k}^{c},$$

where $e_{i,k}$ is the speed error of the i^{th} model at the k^{th} step, y_k is the angular speed of the plant at the k^{th} time step, and $y^{c}{}_{i,k}$ is the angular speed of i^{th} model at the k^{th} step. C_{fe} is the convergence coefficient of the probabilities.

$$W_{i,k} = \frac{P_{i,k}}{\sum_{j=1}^{N} P_{j,k}}. \quad (2)$$

After calculating the weight of each model, in each iteration, the output signals of the controllers are combined and applied to the plant. Therefore, the control signal of each model in each iteration ($u_{j,k}$) is multiplied by its own weight. The multiplications are then added together to create the final control signal. According to the MMC strategy, this hybrid signal (u_j) should be applied to both plant and each of the models in the model bank.

$$u_k = \sum_{i=1}^{N} W_{j,k} \cdot u_{j,k}. \quad (3)$$

2.3. Model Bank. In this study, the plant is a synchronous generator connected to a power system that 8^{th} order model has been used to describe the synchronous generator. To implement the MMC strategy, the expected response space of the system and the machine must be modeled. For this purpose, two 3^{rd} order models for low and medium load conditions of the synchronous generator are considered. These reduced-order models are designed according to the operating point of the synchronous generator in medium load and low load conditions to be able to estimate the dynamic behavior of the synchronous generator at all operating points and in postdisturbance conditions. Each of the models in the model bank is connected to the same power system under study.

2.4. Controller Bank. In the control bank for each of the models in the model bank, a linear optimal controller is designed, as described in the next section. This controller generates two output signals that are applied to the synchronous generator excitation system and static var compensator (SVC) in each model.

3. The Linearized Dynamic Model of the Power System under Study

The 3^{rd} order model of synchronous generator is used as a system linear model in this paper. Also, the synchronous machine excitation system is the IEEE Type-ST1 A [36]. The

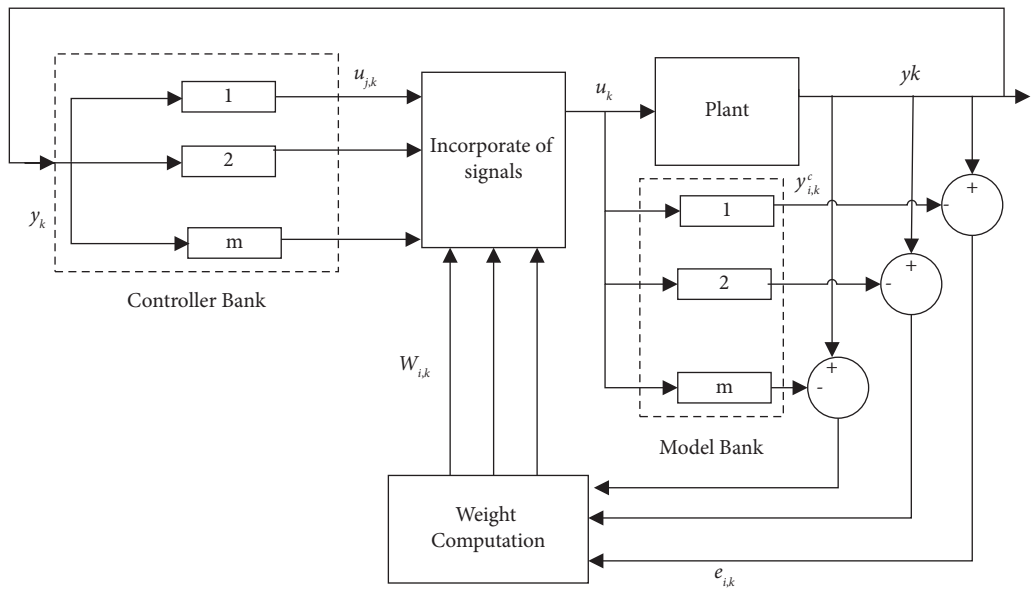

Figure 1: The multiple-model control strategy.

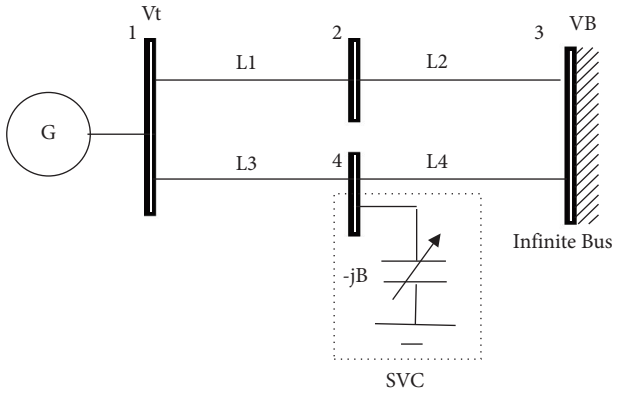

Figure 2: Studied power system.

parameters K_A and T_A are the gain and time constants related to this system, respectively.

$$\frac{d\delta}{dt} = \omega_b(\omega_r - 1),$$
$$\frac{d\omega}{dt} = \frac{(P_m - P_e - D\Delta\omega)}{M}, \tag{4}$$

$$\frac{de'_q}{dt} = \frac{1}{\tau'_{do}}\left[e_{fd} - (x_d - x'_d)i_d - e'_q\right], \tag{5}$$

$$\frac{de_{fd}}{dt} = \frac{1}{T_A}\left[-e_{fd} - K_A(v_{tr} - v_t)\right], \tag{6}$$

where the input electrical power is calculated by

$$P_e = v_{ds}i_{ds} + v_{qs}i_{qs}, \tag{7}$$

where M and D are the inertia constant and damping coefficient, respectively.

3.1. Modeling of the Synchronous Generator. The 8th order synchronous machine model [37] is used for accurate simulation:

$$\frac{d\psi_{qs}}{dt} = \omega_b\left[v_{qs} - \frac{\omega_r}{\omega_b}\psi_{ds} + \frac{r_s}{x_{ls}}(\psi_{mq} - \psi_{qs})\right],$$
$$\frac{d\psi_{ds}}{dt} = \omega_b\left[v_{ds} - \frac{\omega_r}{\omega_b}\psi_{qs} + \frac{r_s}{x_{ls}}(\psi_{md} - \psi_{ds})\right],$$
$$\frac{d\psi_{kq1}}{dt} = \omega_b\left[v_{kq1} - \frac{r_{kq1}}{x_{lkq1}}(\psi_{mq} - \psi_{kq1})\right],$$
$$\frac{d\psi_{kq2}}{dt} = \omega_b\left[v_{kq2} - \frac{r_{kq2}}{x_{lkq2}}(\psi_{mq} - \psi_{kq2})\right], \tag{8}$$
$$\frac{d\psi_{kd}}{dt} = \omega_b\left[v_{kd} - \frac{r_{kd}}{x_{lkd}}(\psi_{md} - \psi_{kd})\right],$$
$$\frac{d\delta}{dt} = \omega_b(\omega_r - 1),$$
$$\frac{d\omega}{dt} = \frac{1}{M}(P_m - P_e - D\Delta\omega),$$

where ψ is the linkage fluxes of different synchronous generator windings, $kq1$, $kq2$, and kd are the indices denoting rotor q and d axis damper windings, and fd denotes the rotor field winding. P_m and P_e are the generator's mechanical and electrical power, respectively, and ω_b is the base angular speed. To obtain control law, the first step is

linearization of the studied power system. In Figure 3, one can see that

$$-I_{ae} + \frac{v_t - v_B}{Z_{\text{line}}} + \frac{v_t - v_C}{Z_{\text{line}}/2} = 0, \tag{9}$$

$$I_{sh} + \frac{v_C - v_B}{Z_{\text{line}}/2} + \frac{v_C - v_t}{Z_{\text{line}}/2} = 0, \tag{10}$$

where Z_{line} is the impedance of each line and in this paper, it is supposed to be $0.015 + j0.175$ pu.

Substituting $v_t = v_d + jv_q$ and $Z_{\text{line}} = R + jX$ in (9) and (10) and separating imaginary and real parts result in

$$\begin{aligned} v_t &= v_B - \frac{1}{4}(Z_{\text{line}} \cdot I_{sh}) + \frac{1}{2}(Z_{\text{line}} \cdot I_{ae}), \\ v_d &= v_B \cdot \cos\delta - \frac{X}{4}|I_{sh}| + \frac{1}{2}R \cdot i_d - \frac{1}{2}X.i_q, \\ v_q &= v_B \cdot \sin\delta - \frac{R}{4}|I_{sh}| + \frac{1}{2}X \cdot i_d - \frac{1}{2}X.i_q. \end{aligned} \tag{11}$$

Now, the obtained v_d and v_q are placed in the machine's model equations (37) and then equations i_d and i_q are obtained from δ, e'_q, and I_{sh} and subsequently the resulting equations have been linearized:

$$\begin{aligned} \begin{bmatrix} v_q \\ v_d \end{bmatrix} &= \begin{bmatrix} 1 \\ 0 \end{bmatrix} e'_q - \begin{bmatrix} 0 & x'_d \\ -x_q & 0 \end{bmatrix} \begin{bmatrix} i_q \\ i_d \end{bmatrix}, \\ \begin{bmatrix} \Delta i_q \\ \Delta i_d \end{bmatrix} &= \begin{bmatrix} D_q & -E_q & L_q \\ D_d & -E_d & L_d \end{bmatrix} \begin{bmatrix} \Delta\delta \\ \Delta e'_q \\ \Delta I_{sh} \end{bmatrix}, \end{aligned} \tag{12}$$

where D_q, D_d, E_q, E_d, L_q, and L_d all are functions of R, X, V_B, x'_d, x_q, and δ_0. Next, the linearized 3rd order model of a synchronous machine is used to obtain the state-space equations:

$$p\Delta\delta = \omega_b \Delta\omega_r, \tag{13}$$

$$p\Delta\omega_r = \frac{1}{M}(\Delta P_m - \Delta P_e). \tag{14}$$

Substituting linear electrical power equations in (26) results in [37]

$$\begin{aligned} p\Delta\omega_r &= \frac{1}{M}\left[\Delta P_m - K_1\Delta\delta - K_2\Delta e'_q - K_p\Delta I_{sh}\right], \\ K_1 &= \left[\left(x_q - x'_d\right)i_{d_0} + e'_{q_0}\right]D_q + \left(x_q - x'_d\right)i_{q_0}D_d, \\ K_2 &= -\left[\left(x_q - x'_d\right)i_{d_0} + e'_{q_0}\right]E_q - \left(x_q - x'_d\right)i_{q_0}E_d + i_{q_0}, \\ K_p &= \left[\left(x_q - x'_d\right)i_{d_0} + e'_{q_0}\right]L_q + \left(x_q - x'_d\right)i_{q_0}L_d. \end{aligned} \tag{15}$$

Considering the excitation system of Figure 4, linearization of (5) results in

$$p\Delta e'_q = \frac{1}{\tau'_{do}}\left[\Delta e_{fd} - K_4\Delta\delta - K_3\Delta e'_q - K_q\Delta I_{sh}\right], \tag{16}$$

$$\begin{aligned} K_3 &= 1 - (x_d - x'_d)E_d, \\ K_4 &= (x_d - x'_d)D_d, \\ K_q &= (x_d - x'_d)L_d. \end{aligned} \tag{17}$$

$$p\Delta e_{fd} = \frac{1}{T_A}\left[-\Delta e_{fd} + K_A\left(-\Delta v_t + u_E\right)\right], \tag{18}$$

$$p\Delta e_{fd} = \frac{1}{T_A}\left[-\Delta e_{fd} + K_A\left(-K_5\Delta\delta - K_6\Delta e'_q - K_v\Delta I_{sh} + u_E\right)\right], \tag{19}$$

$$\begin{aligned} K_5 &= x_q D_q \sin\delta_0 - x'_d D_d \cos\delta_0, \\ K_6 &= -x_q E_q \sin\delta_0 + (1 + x'_d E_d)\cos\delta_0, \\ K_v &= x_q L_q \sin\delta_0 - x'_d L_d \cos\delta_0. \end{aligned} \tag{20}$$

Defining $X = [\Delta\delta\ \Delta\omega\ \Delta e'_q\ \Delta e_{fd}]^T$ as the state vector and $u = [u_E I_{sh}]^T$, from (13), (15), (16), and (19), the system state-space can be expressed as follows:

$$\dot{X} = AX + Bu, \tag{21}$$

where

$$\begin{aligned} A &= \begin{bmatrix} 0 & \omega_b & 0 & 0 \\ \frac{-K_1}{M} & 0 & \frac{-K_2}{M} & 0 \\ \frac{-K_4}{\tau'_{\text{do}}} & 0 & \frac{-K_3}{\tau'_{\text{do}}} & \frac{1}{\tau'_{\text{do}}} \\ \frac{-K_A K_5}{T_A} & 0 & \frac{-K_A K_6}{T_A} & \frac{-1}{T_A} \end{bmatrix}, \\ B &= \begin{bmatrix} 0 & 0 \\ 0 & \frac{-K_v}{M} \\ 0 & \frac{-K_q}{\tau'_{do}} \\ \frac{K_A}{T_A} & \frac{-K_A K_v}{T_A} \end{bmatrix}. \end{aligned} \tag{22}$$

4. Linear Optimal Control Approach

The LOC theory described in [33–35] is restated in this section briefly. In the LOC method, by defining the energy function J as in (23), and minimizing that the optimal linear control signal u according to the feedback control law is obtained:

$$J = \frac{1}{2}\int_{t_0}^{t_f}\left(X^T QX + u^T Ru\right)\mathrm{d}t, \tag{23}$$

$$u = -R^{-1}B^T KX. \tag{24}$$

In (23), the weight R is the real, definite positive and symmetric matrix and the Q is the real, symmetric positive, and quasidefinite weight matrix. In this paper, they selected as follows:

$$R = \begin{bmatrix} 1 & 0 \\ 0 & 1 \end{bmatrix},$$
$$Q = \begin{bmatrix} 100 & 0 & 0 & 0 \\ 0 & 1000 & 0 & 0 \\ 0 & 0 & 0.1 & 0 \\ 0 & 0 & 0 & 0 \end{bmatrix}. \tag{25}$$

The matrix K is obtained by solving the Riccati equation given in (26). Substituting the optimal K in (24), the optimal u is calculated. It generates the optimal control signal for controlling the excitation system and SVC simultaneously:

$$A^T K + KA - KBR^{-1}K^T + Q = 0. \tag{26}$$

5. Results and Discussion

The power system shown in Figure 2 and the proposed MMLOC shown in Figure 1 is simulated using MATLAB®. The simulation code is built in MATLAB/m-code environment using a step size 0.1 ms. The 4th order Runge-Kutta numerical method is used to solve the 8th order synchronous generator nonlinear equations (as the real plant) and the third order of synchronous generator nonlinear equations (as the models) and the power system. The parameters of the synchronous generator can be found in Table 1. To investigate the effect of the MMLOC strategy, it is assumed that a three-phase symmetric fault has occurred in the middle of lines 1–3 in the scenario of Table 2.

The aim of this paper is to damp LFO via applying coordinated control to the generator excitation system and SVC. Hence, the postfault dynamics of the synchronous generator have been estimated by the multimodel approach and the LOC method has been used for the production of control signals. Each model produces its own optimal linear control signal. Combining the control signals of the models together probabilistically, the final control signals are generated and applied to the plant. To evaluate the performance of the MMLOC strategy, this strategy has been compared with the SM control method and comparative results have been drawn in Figures 5 and 6. To better compare the MMLOC and SMC performances, the coefficients of the SMC method have been adjusted so that the excitation voltage diagram and the terminal voltage in both methods are superimposed. The results are shown in Figures 7 and 8. Also, the generator output current has the same maximum values, which are shown in Figure 9. As in the more detailed figures drawn in Figures 7 and 9, it can be seen that the SMC method causes a lot of chattering in the voltage and current of the generator, which is a big disadvantage for the SMC control method. The final control signals contain the excitation voltage (E_{xfd}) and the SVC susceptance (B_{svc}) that are drawn in Figures 8 and 10, respectively. The control performance of rotor speed based on MMLOC, SM, and no control are shown in Table 3. It

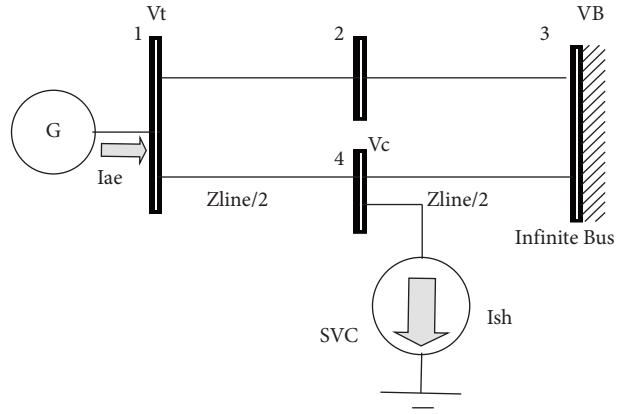

Figure 3: The power system model under study.

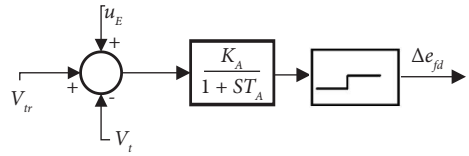

Figure 4: The exciter system model.

Table 1: The synchronous generator parameters.

Parameters	Value (pu)
D	0.01
r_s	0.0019
x_{ls}	0.19
x_d	1.8
x_q	1.8
x_{lfd}	0.1414
r_{fd}	0.000929
x_{lkd}	0.08125
r_{kdK}	0.01334
x_{lkq1}	0.8125
r_{kq1}	0.00178
x_{lkq2}	0.0939
r_{kq2}	0.00841

Table 2: Three-phase fault planning.

Step	Plan	Time (sec)
1	Steady state	$t < 0.5$
2	There is a 3-phase fault in the middle of lines 1–3	$0.5 < t < 0.7$
3	Lines 1–3 is opened on both sides	$0.7 < t < 1.7$
4	The fault is removed and the lines 1–3 are reclosed	$t > 1.7$

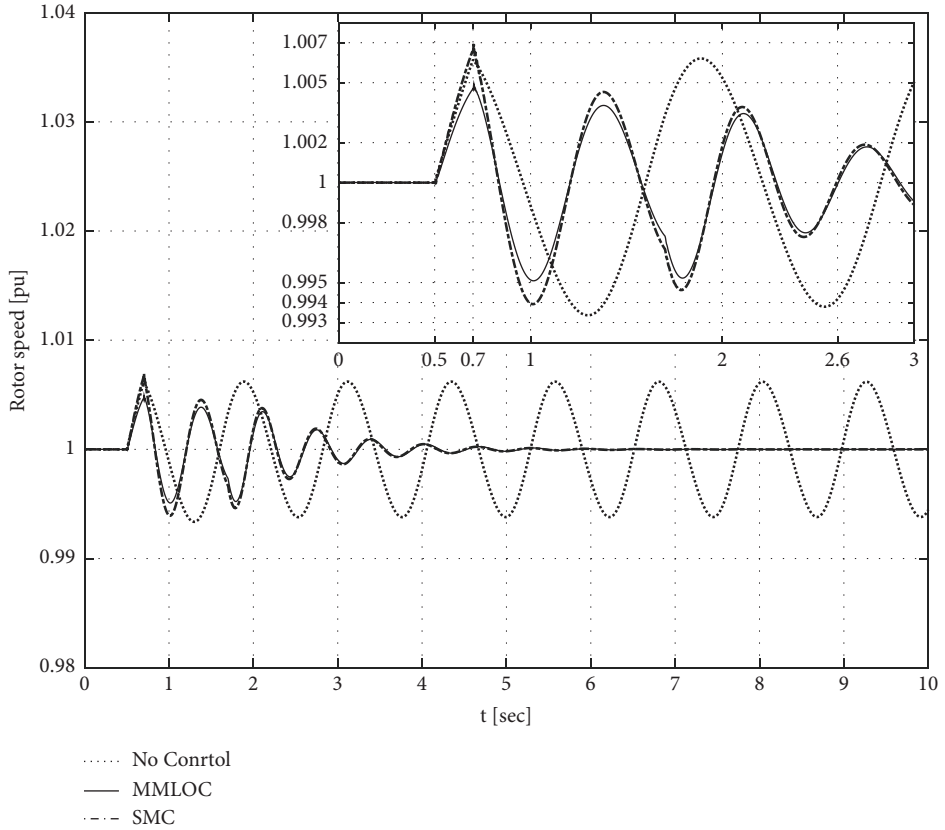

Figure 5: Rotor speed of the generator with MMLOC and SMC and without control.

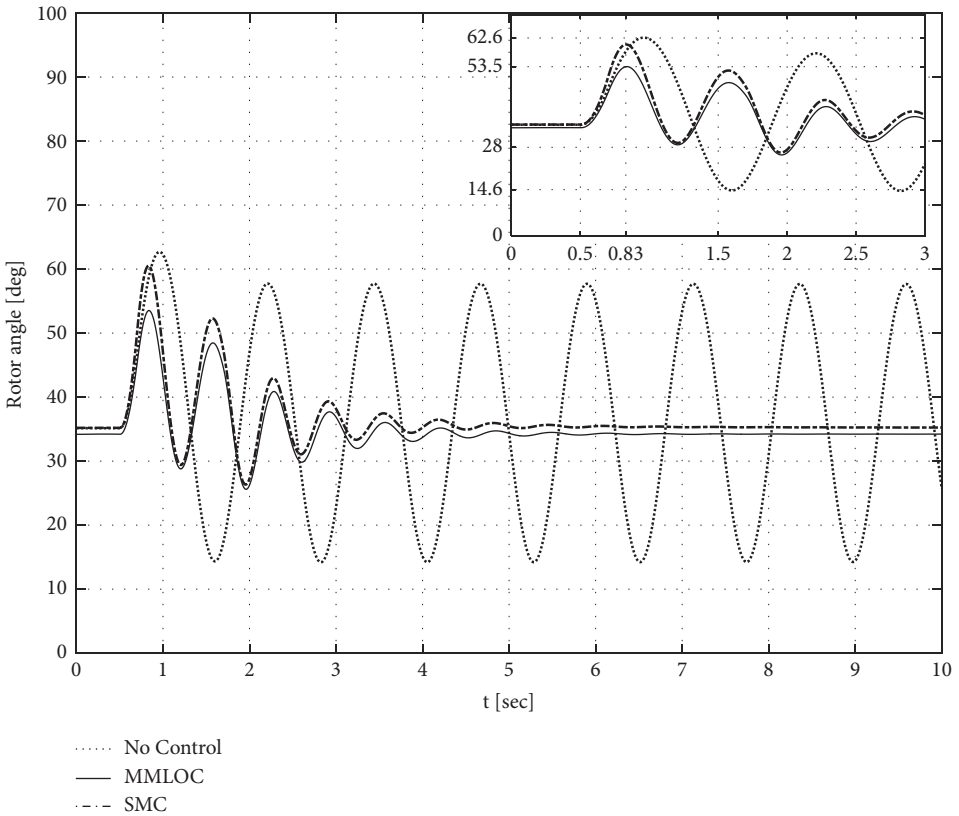

Figure 6: Rotor angle of the generator with MMLOC and SMC and without control.

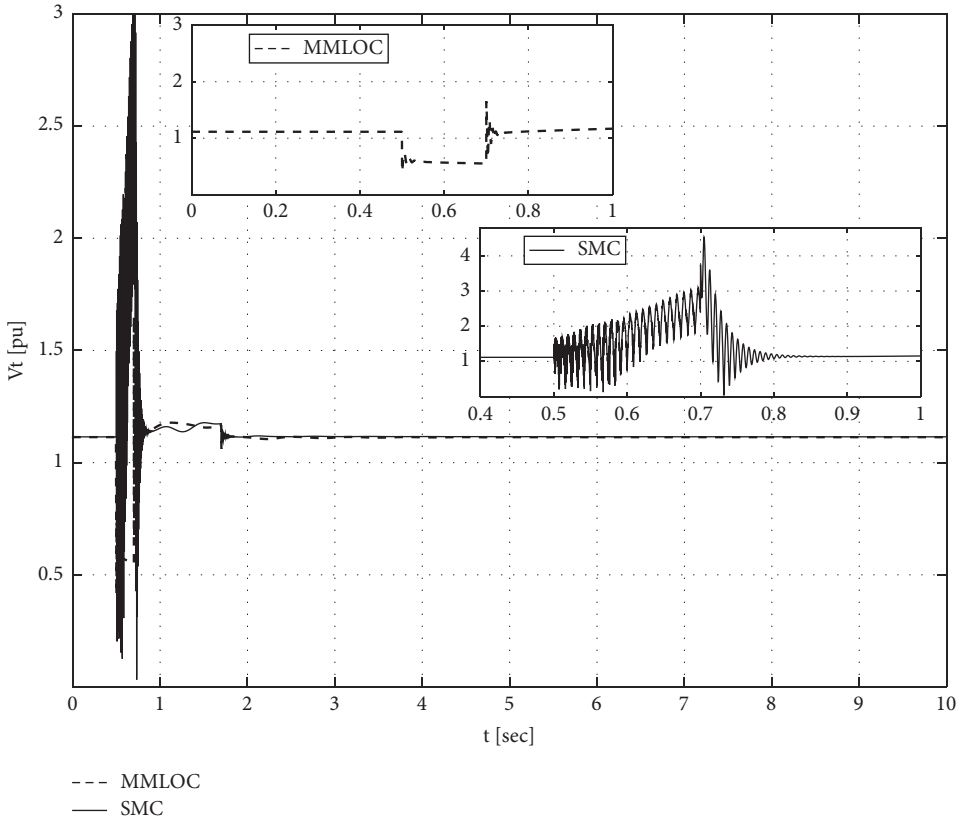

Figure 7: Terminal voltage of the generator with MMLOC and SMC.

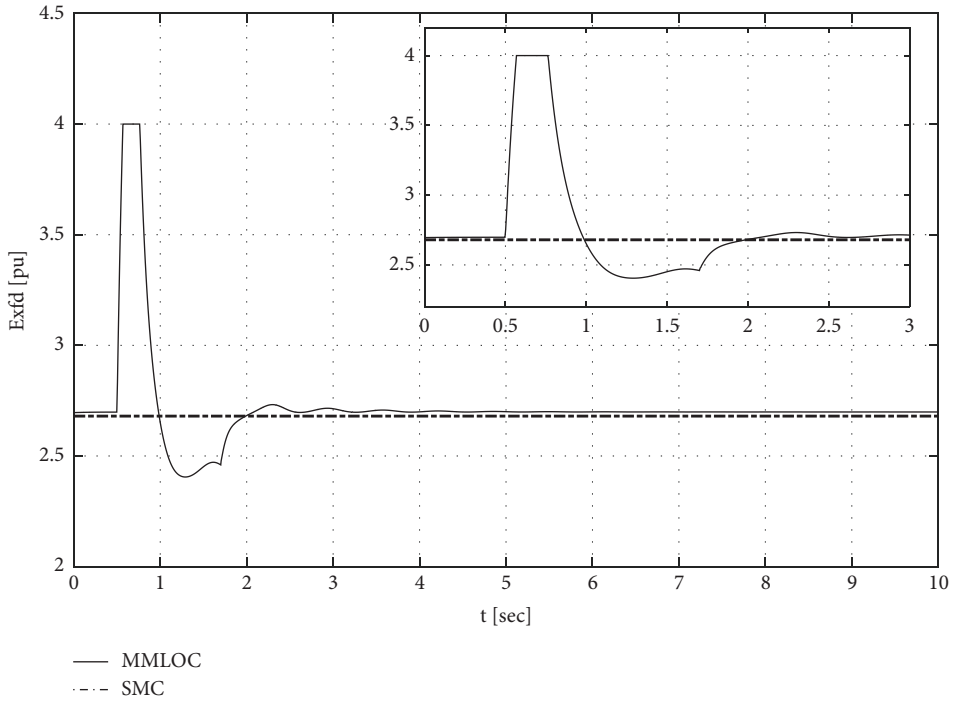

Figure 8: Exciter voltage of the generator with MMLOC and SMC.

can be seen that the control performances of MMLOC and SM are much better than no control. There are the lower peak and the lower valley in MMLOC compared with those of SM strategy. The rise time is the same in both control methods because the three-phase fault has not yet been seen by the controller.

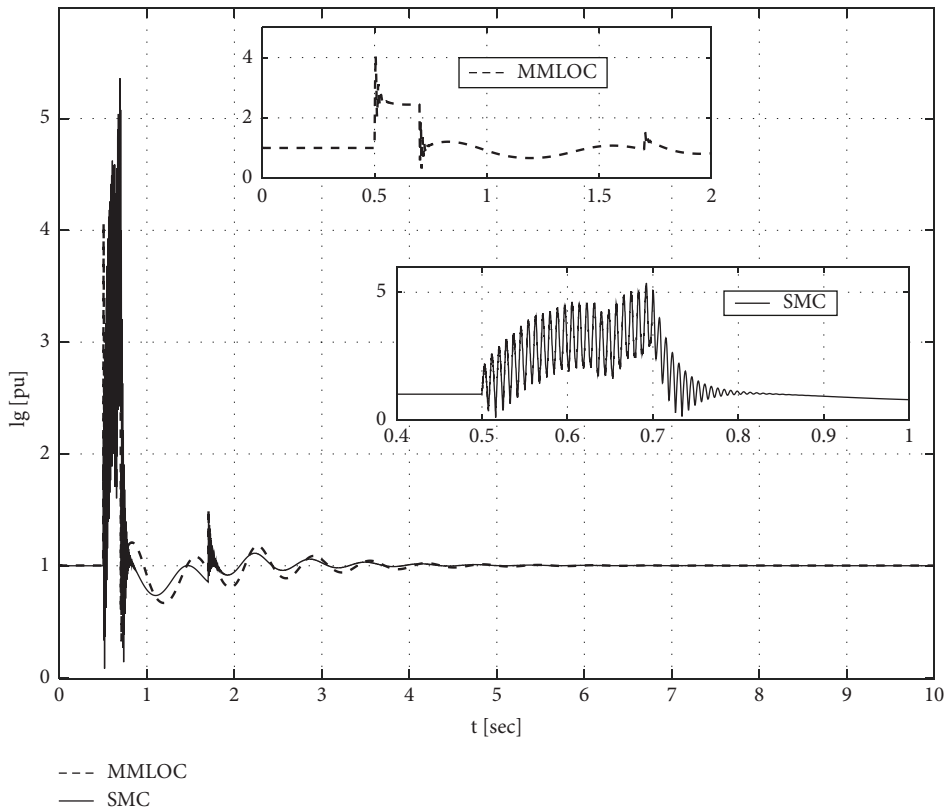

Figure 9: The current generator with MMLOC and SMC.

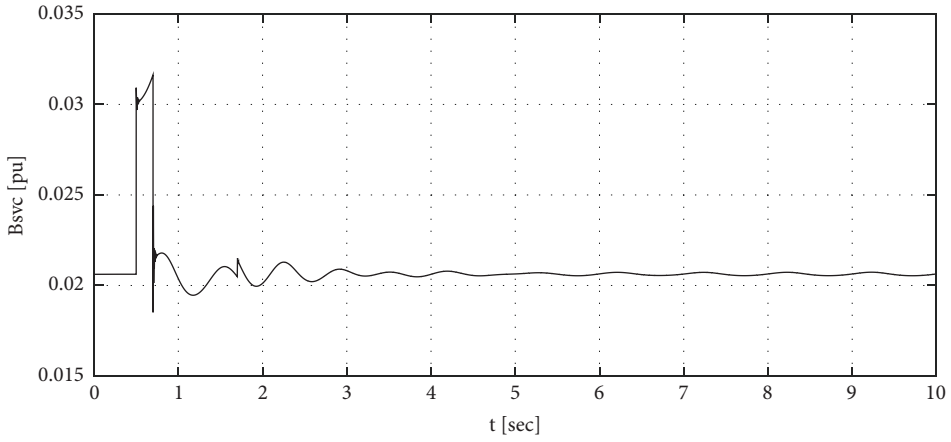

Figure 10: The control signal of SVC in MMLOC strategy.

Table 3: The performance index rotor speed under three-phase fault.

Control strategy	Peak (pu)	Valley (pu)	Rise time (s)	Settling time (s)
MMLOC	1.005	0.995	0.7	2
SMC	1.007	0.994	0.7	2
No control	1.007	0.993	0.7	>10

Table 4: The performance index rotor angle under three-phase fault.

Control strategy	Peak (pu)	Valley (pu)	Rise time (s)	Settling time (s)
MMLOC	53.5	28	0.83	2
SMC	62	28	0.83	2
No control	62.6	14.6	0.96	>10

The control performance of rotor angle based on MMLOC, SM, and no Control are shown in Table 4. It can be seen that the control performances of MMLOC and SM are much better than no control. There is the lower peak in MMLOC compared with that of SM strategy. Similarly, the rise time is the same in both control methods because the

three-phase fault has not yet been seen by the controller. Also, the settling time is almost the same in both methods and both performance index [38–42].

Data Availability

The datasets generated during and/or analyzed during the current study are available from the corresponding author on reasonable request.

Disclosure

This research was done at Islamic Azad University, for a Ph. D. thesis.

Conflicts of Interest

The authors declare that they have no conflicts of interest regarding the publication of this paper.

References

[1] A. Ulbig, T. S. Borsche, and G. Andersson, "Impact of low rotational inertia on power system stability and operation," *IFAC Proceedings Volumes*, vol. 47, no. 3, pp. 7290–7297, Aug, 2014.

[2] Y. Xue and Z. Bin, "Analysis of mode interaction in ultra-low-frequency oscillation based on trajectory eigenvalue," *Journal of Modern Power Systems and Clean Energy*, vol. 8, no. 6, pp. 1208–1220, Nov, 2020.

[3] W. Wang, L. Jiang, Y. Cao, and Y. Li, "A parameter alternating VSG controller of VSC-mtdc systems for low-frequency oscillation damping," *IEEE Transactions on Power Systems*, vol. 35, no. 6, pp. 4609–4621, 2020.

[4] M. Zarifakis, D. J. Byrne, W. T. Coffey, Y. P. Kalmykov, S. V. Titov, and S. J. Carrig, "Comparison of coupled nonlinear oscillator models for the transient response of power generating stations connected to low inertia systems," *IEEE Transactions on Power Systems*, vol. 35, no. 1, pp. 795–802, 2020.

[5] L. Wang, C. H. Chang, B. L. Kuan, and A. V. Prokhorov, "Stability improvement of a two-area power system connected with an integrated onshore and offshore wind farm using a STATCOM," *IEEE Transactions on Industry Applications*, vol. 53, no. 2, pp. 867–877, 2017.

[6] U. Markovic, O. Stanojev, P. Aristidou, E. Vrettos, D. Callaway, and G. Hug, "Understanding small-signal stability of low-inertia systems," *IEEE Transactions on Power Systems*, vol. 36, no. 5, pp. 3997–4017, 2021.

[7] T. Guesmi, B. M. Alshammari, Y. Almalaq, A. Alateeq, and K Alqunun, "New coordinated tuning of SVC and PSSs in multimachine power system using Coyote optimization algorithm," *Sustainability*, vol. 13, no. 6, p. 3131, 2021.

[8] B. Dasu, M. Sivakumar, and R. Srinivasarao, "Interconnected multi-machine power system stabilizer design using whale optimization algorithm," *Protection and Control of Modern Power Systems*, vol. 4, no. 1, p. 2, 2019.

[9] J. Morsali and T. ghanizadehboland, "Proposing FOPID-Based PSS2B Stabilizer Using MGSO to Improve Damping of Electromechanical Oscillations in a Multi-Machine Power System," in *Proceedings of the 27th Iranian Conference on Electrical Engineering*, ICEE, Yazd, Iran, May 2019.

[10] S. Jalali and GH. Shahgholian, "Designing of power system stabilizer based on the root locus method with lead-lag controller and comparing it with PI controller in multi-machine power system," *Journal of Power Technologies*, vol. 98, no. 1, pp. 45–56, 2018.

[11] W. Du, W. Dong, Y. Wang, and H. F. Wang, "A method to design power system stabilizers in a multi-machine power system based on single-machine infinite-bus system model," *IEEE Transactions on Power Systems*, vol. 36, no. 4, pp. 3475–3486, 2021.

[12] C. Abdelghani, L. Chaib, and S. Arif, "Robust control design of PSS for dynamic stability enhancement of power system," *Journal of Electrical Systems*, vol. 13, no. 2, pp. 376–386, 2017.

[13] K. Sebaa, Y. Zhou, Y. Li, A. Gelen, and H. Nouri, "Low-frequency oscillation damping control for large-scale power system with simplified virtual synchronous machine," *Journal of Modern Power Systems and Clean Energy*, vol. 9, no. 6, pp. 1424–1435, 2021.

[14] Z. Bin and Y. Xue, "A method to extract instantaneous features of low-frequency oscillation based on trajectory section eigenvalues," *Journal of Modern Power Systems and Clean Energy*, vol. 7, no. 4, pp. 753–766, 2019.

[15] A. Mostajabi, Sh. Shojaeian, and M. Lotfi, "Improving low-frequency oscillation damping of a multi-area power system using multi-model adaptive control approach," *International Journal of Mechatronics, Electrical and Computer Technology*, vol. 4, no. 11, pp. 628–646, 2014.

[16] R. R. Rao, B. Aufderheide, and B. W. Bequette, "Experimental studies on multiple model predictive control for automated regulation of hemodynamic variables," *IEEE Transactions on Biomedical Engineering*, vol. 50, no. 3, pp. 277–288, 2003.

[17] A. Abdlrahem and H. Albalawi, "A multi-model approach to design a robust SVC damping controller using convex optimization technique to enhance the damping of inter-area oscillations considering time delay," *Energy and Power Engineering*, vol. 09, no. 12, pp. 750–771, Jan 2017.

[18] L. Zhou, X. Yu, B. Li et al., "Damping inter-area oscillations with large-scale PV plant by modified multiple model adaptive control strategy," *IEEE Transactions on Sustainable Energy*, vol. 8, no. 4, pp. 1629–1636, Oct, 2017.

[19] Sh. Shojaeian and J. Soltani, "Low-frequency oscillations damping of a power system including unified power flow controller based on adaptive back stepping control," *Automatique et ordinateurs*, vol. 58, no. 2, 2013.

[20] E. Sharifi and A. H. Mazinan, "On transient stability of multi-machine power systems through Takagi–Sugeno fuzzy-based sliding mode control approach," *Complex Intell. Syst*, vol. 4, no. 3, pp. 171–179, Nov 2017.

[21] M. Azizi, "Designing of a fuzzy-sliding mod controller for UPFC to improve the transient stability," *Majlesi Journal of Mechatronic Systems*, vol. 6, no. 1, 2017.

[22] S. Huang, L. Xiong, J. Wang, P. Li, Z. Wang, and M. Ma, "Fixed-time fractional-order sliding mode controller for multi machine power systems," *IEEE Transactions on Power Systems*, vol. 36, no. 4, pp. 2866–2876, 2021.

[23] R. K. Patnaik and S. P. Mishra, "Adaptive fractional integral terminal sliding mode power control of UPFC in DFIG wind farm penetrated multi machine power sys," *Protection and Control of Modern Power Systems*, vol. 3, no. 8, 2018.

[24] A. S. L. V. Tummala, R. Inapakurthi, and P. V. Ramanarao, "Observer based sliding mode frequency control for multi-machine power systems with high renewable energy," *Journal of Modern Power Systems and Clean Energy*, vol. 6, no. 3, pp. 473–481, 2018.

[25] M. Ouassaid, M. Maaroufi, and M. Cherkaoui, "Observer-based nonlinear control of power system using sliding mode control strategy," *Electric Power Systems Research*, vol. 84, no. 1, pp. 135–143, 2012.

[26] A. T. Tran, B. L. N. Minh, V. V. Huynh et al., "Load frequency regulator in interconnected power system using second-order sliding mode control combined with state estimator," *Energies*, vol. 14, no. 4, pp. 863–2021, 2021.

[27] X. Liu and Y. Han, "Decentralized multi-machine power system excitation control using continuous higher order sliding mode technique," *International Journal of Electrical Power & Energy Systems*, vol. 82, pp. 76–86, 2016.

[28] Y. Chen, H. Wang, M. Zhu, M. Liu, J. Ma, and X. Cai, "Passive sliding mode controlled UPFC and its treatment strategy of unbalanced grid conditions," *Frontiers in Energy Research Key Laboratory of Control of Power Transmission and Conversion*, vol. 9, Ministry of Education, Shanghai Jiao Tong University, Shanghai, China, July 2021.

[29] Zh. Liu, Sh. Liu, Zh. Li, and I. Adamu Tasiu, "A Novel Approach Based on Extended State Observer Sliding Mode Control to Suppress Voltage Low-frequency Oscillation of Traction Network," *IEEE Access*, vol. 7, pp. 52440–52454, 2019.

[30] K. Liao, Y. Xu, and H. Zhou, "A robust damping controller for DFIG based on variable-gain sliding mode and Kalman filter disturbance observer," *International Journal of Electrical Power & Energy Systems*, vol. 107, pp. 569–576, 2019.

[31] Ch. Abdelghani, Ch. Lakhdar, and A. Salem, "Incorporation of sliding mode control and PID for dynamic stability enhancement of power system," in *Proceedings of the International Conference on Recent Advances in Electrical Systems*, Tunisia, 2016.

[32] C. C. Soon, R. Ghazali, H. I. Jaafar, and S. Y. S. Hussien, "Sliding mode controller design with optimized PID sliding surface using particle swarm algorithm," *Procedia Computer Science*, vol. 105, pp. 235–239, 2017.

[33] H. Abniki, A. Asadi, P. Khajavi, and M. T. Nabavi-Razavi, "Novel Optimization Technique for Linear Optimal Control and Power System Stabilizer in Multi-Machine Power Systems," *A*, in *Proceedings of the 10th International Conference on Environment and Electrical Engineering*, Rome, Italy, May 2011.

[34] Y.-N. Yu, *Electric Power System Dynamics*, Academic Press, Cambridge, USA, 1983.

[35] R. Fazal and M. A. Choudhry, "Design of non-linear static var compensator based on synergetic control theory," *Electric Power Systems Research*, vol. 151, pp. 243–250, 2017.

[36] P. Kundur, *Power System Stability and Control*, McGraw-Hill, New York, USA, 1994.

[37] P. C. Krause, O. Wasynczuk, and S. D. Sudhoff, *Analysis of Electric Machinery*, McGraw-Hill, New York, USA, 2002.

[38] A. R. Sobbouhi and A. Vahedi, "Transient stability prediction of power system; a review on methods classification and considerations," *Electric Power Systems Research*, vol. 190, p. 106853, 2021.

[39] M. E. C. Bento, R. A. Ramos, and S. Carlos, "A method based on linear matrix inequalities to design a wide-area damping controller resilient to permanent communication failures," *IEEE Systems Journal*, vol. 15, no. 3, pp. 3832–3840, 2021.

[40] C. O. Maddela and B. Subudhi, "Robust wide-area TCSC controller for damping enhancement of inter-area oscillations in an interconnected power system with actuator saturation," *International Journal of Electrical Power & Energy Systems*, vol. 105, pp. 478–487, 2019.

[41] B. V. Patil, L. Sampath, A. Krishnan, and F. Y. Eddy, "Decentralized nonlinear model predictive control of a multimachine power system," *International Journal of Electrical Power & Energy Systems*, vol. 106, pp. 358–372, 2019.

[42] M. Saadatmand, B. Mozafari, G. B. Gharehpetian, and S. Soleymani, "Optimal damping controller design for large-scale PV farms to damp the low-frequency oscillation," *International Journal of Renewable Energy Resources*, vol. 9, no. 4, pp. 1672–1680, 2019.